Broadband and High-Gain Circularly-Polarized Antenna With Low RCS

Saman Zarbakhsh, *Student Member, IEEE*, Mohammad Akbari, *Member, IEEE*, Fereshteh Samadi, *Student Member, IEEE*, and Abdel-Razik Sebak, *Fellow, IEEE*

***Abstract*— In this paper, a wideband circularly polarized (CP) antenna with a low radar cross section (RCS) and high gain properties is investigated. The proposed antenna is based on a combination of the Fabry–Perot cavity (FPC) and sequential feeding technique. The purpose of this antenna is to produce CP with high directive gain over a wide bandwidth while preserving low RCS. The principle of the FPC and resonance is achieved by applying one frequency selective surface (FSS) metasurface. A microstrip slot array operating at the Ka-band, excited by a sequentially rotated feeding network, is designed and fabricated. It is indicated that all the merits mentioned above can be obtained over a broad frequency band by designing a suitable FSS metasurface and modifying the feeding lengths to adjust desirable phase. RCS reduction is realized by 180° ± 37° reflection phase variations between adjacent FSS unit cells on the metasurface. The experimental results show that the gain of the antenna with the metasurface is at least 7 dB greater than that of the primary antenna with a peak value approximately 20 dB at 28.5 GHz. In addition, bandwidths of 3-dB gain, impedance (|S11| ≤ −10 dB), and axial ratio ≤3 dB are ranged from 27.5 to 33.5 GHz (19.7%), 26.7 to 34.2 GHz (24.6%), and 26.8 to 33.1 GHz (21%), respectively. The monostatic RCS reduction for a normal incidence is effectively suppressed from 28 to 48 GHz (52%).**

***Index Terms*— Antenna, circularly polarization (CP), Fabry–Perot cavity (FPC), frequency selective surface (FSS), metasurface, radar cross section (RCS), sequential feeding.**

I. Introduction

IN RADAR and satellite industries, in which both high-directive and circular-polarized (CP) antennas are essential, the Fabry–Perot cavity (FPC) approach can be a suitable choice due to some advantages such as radiation characteristics and compact structure. FPC antenna (FPCA) usually consists of a primary radiator embedded inside a cavity formed by locating a nearly half a wavelength metasurface above a metal ground plate. With interesting merits of high-gain and simple feeding, FPCA has recently attracted considerable interest [1]–[16].

From the standpoint of the radiator, two methods can be employed to realize CP-FPCA: 1) adding a metasurface on the top of a CP feeding antenna [6], [7] and 2) placing a metasurface on the top of a linearly polarized (LP) feed which usually rotates by 45° with respect to the axes [17]–[21]. In 1), a metasurface is applied to shape an FPC while the CP feeding network is needed and essential [6], [7]. In 2), the metasurface should carry out two functions at the same time: one is to shape the FPC integration with the ground plate and the second one is to behave as a polarizer structure to transform the LP radiation of the feed into a CP one. However, both methods in previous work suffer from some drawbacks including restricting both CP bandwidth and gain enhancement [1]–[16].

High-gain CP antennas with low radar cross section (RCS) have received critical attention for some stealth platforms to mitigate the issue of polarization mismatch losses between the transmitting and receiving antennas. A scheme to design a high-gain and low-RCS antenna by using an FPC has been given in [22] and [23]. In these designs, resistors are used on the metasurface to suppress the backward RCS by absorbing energy in the incoming electromagnetic (EM) waves. However, it is difficult to implement the antenna with a large number of welded resistors. In [25], a reconfigurable metasurface absorber is used to control and reduce the RCS property for CP or LP antenna. A low-RCS CP antenna array using another technique including a random phase distribution of the elements is presented in [26]. However, antennas based on these techniques have limited frequency bandwidth. The frequency band along with the maximum value of RCS suppression is controlled by optimizing the polarization conversion band and the polarization conversion ratio, respectively, in [27]. However, to keep away from the degradation of antenna radiation performance, the in-band RCS has not been suppressed in [27]. As compared with previously published works in the open literature, this paper main contribution is to present a low-profile one-layer metasurface high-gain FPCA with simultaneous properties of broadband CP, impedance matching, and low RCS.

In order to achieve such high combined performance, a new kind of broadband high-gain CP FPCA with low-RCS is introduced in this paper by employing a frequency selective surface (FSS) metasurface. The wideband RCS reduction (52%) is realized by 180° ± 37° reflection phase variations between adjacent FSS unit cells on the metasurface. By correct employment of an FPC approach, a gain enhancement of at least 7 dB is achieved. In addition, the 3 dB gain bandwidth is nearly 19.7%. A 21% wide axial ratio (AR) bandwidth

Manuscript received February 18, 2018; revised August 24, 2018; accepted September 17, 2018. Date of publication October 16, 2018; date of current version January 16, 2019. *(Corresponding author: Saman Zarbakhsh.)*

The authors are with the Department of Electrical and Computer Engineering, Concordia University, Montreal, QC H3G 1M8, Canada (e-mail: samanzarbakhsh@yahoo.com; akbari.telecom@gmail.com; fereshteh.samadi16@gmail.com; abdo@ece.concordia.ca).

Color versions of one or more of the figures in this paper are available online at http://ieeexplore.ieee.org.

Digital Object Identifier 10.1109/TAP.2018.2876234

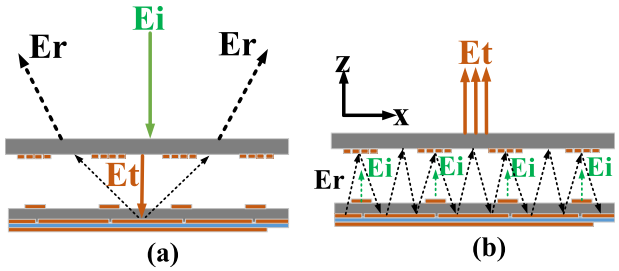

Fig. 1. Schematic of the proposed structure including the antenna with the FSS metasurface for two cases of (a) RCS reduction and (b) gain enhancement.

is attained by the improved polarization purity using both a sequentially rotated feeding network and the phase adjustment of FSS unit cells on the metasurface. Moreover, the primary antenna without the metasurface is broadband (24.4%). Since the FSS metasurface is placed nearly half a wavelength above a metal ground plate, therefore, the proposed integrated structure is broadband (more than 24%), as well.

II. Modeling and Analysis

The proposed FPCA is first analyzed with the ray theory method [28], which is useful in realizing the antenna gain increase and RCS reduction. The FPCA considered in this paper consists of two reflectors and a small printed patch antenna. One of the two reflectors is the FSS metasurface used as a transmitting window, which allows partial transmission of the EM wave and named as a partially reflective surface (PRS). As depicted in Fig. 1(a), the schematic of the proposed FPCA for the purpose of RCS reduction is given. It is observed that the incident waves transmit through the metasurface, air gap, and the antenna's second substrate and then is reflected by the ground plate. Therefore, the operating principle of RCS suppression relies on destructive interference which is arranged by the combination of two kinds of FSS unit cells and FPC. It means that the interaction unit cells are considered as one box containing the metasurface, air gap, second substrate, and metal ground plate (see Fig. 4). With respect to Fig. 1(a), the incident field ($E_{\rm i}$) is equal to the sum of transmitted field ($E_{\rm t}$) and reflected field ($E_{\rm r}$) which is given as $E_{\rm i} = E_{\rm r} + E_{\rm t}$, where $E_{\rm r} = |E_{\rm r}|e^{{\rm j}\varphi_{\rm r}}$ and $E_{\rm t} = |E_{\rm t}|e^{{\rm j}\varphi_{\rm t}}$. Here, due to two kinds of FSS unit cells, reflected field is formed as $E_{\rm r} = E_{\rm r1} + E_{\rm r2}$, where $E_{\rm r1} = |E_{\rm r1}|e^{{\rm j}\varphi_{\rm r1}}$ and $E_{\rm r2} = |E_{\rm r2}|e^{{\rm j}\varphi_{\rm r2}}$. Therefore, the reflected waves produced by FSS #1 and FSS #2 generate destructive interference in the specular direction once $|\varphi_{\rm r1} - \varphi_{\rm r2}|$ is satisfying $(180^\circ \pm 37^\circ)$ as it is acceptable for low-RCS requirements. Moreover, the criteria of $(180^\circ \pm 37^\circ)$ rely on a compromise of in-band and out-of-band RCS suppression. On the other hand, we should fulfill conditions related to the FSS metasurface or PRS. When the FSS metasurface is located at a resonant air gap (cavity height) from the source antenna which itself is backed by a ground plate, the antenna gain is increased considerably, as shown in Fig. 1(b).

The radiated rays by the source antenna are reflected multiple times with reducing amplitudes between the metasurface and the ground plane [see Fig. 1(b)]. These multiple reflections result in constructive interference and increase considerably in the antenna gain along the boresight once the air gap "h" between the antenna ground plate and the metasurface corresponds to [1]

$$h = \frac{\lambda}{4\pi}((\varphi) - 2N\pi) \tag{1}$$

$$\varphi = \varphi_{\rm sub,airgap} + \varphi_{FSS} \tag{2}$$

where φ and λ are the reflection phase of FPC and free space wavelength, respectively. N is an integer and the order of resonant mode (N = 0, 1, 2, ...). Moreover, as N is increasing the sidelobe levels (SLLs) become higher.

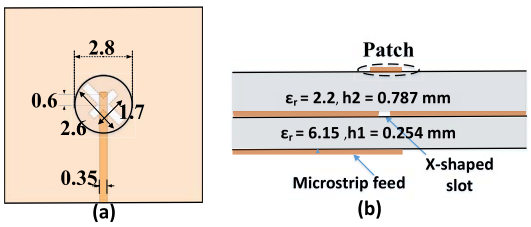

Fig. 2. Geometry of patch antenna. (a) Top view. (b) Side view [29].

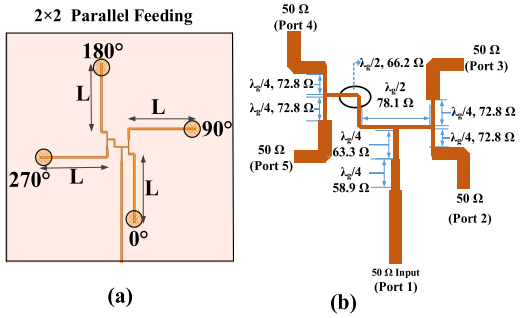

Fig. 3. Sequential feeding network. (a) 2×2 antenna subarrays. (b) Parallel feeding (RHCP) [29] (L = 12 mm).

III. Antenna Design

The geometry of a two-layer single-element antenna fed by aperture coupling is shown in Fig. 2. It consists of two substrates: the bottom substrate is Rogers RO3006 (εr1 = 6.15 and h1 = 0.254 mm), while the top one is Rogers RT/duroid 5880 (εr2 = 2.2 and h2 = 0.787 mm) with an X-shaped slot etched off the common ground plane [29]. As shown in Fig. 3, a parallel feeding technique as one of the sequential feeding networks is given. This structure is based on the architecture presented by Akbari *et al.* [29]. The feeding network is an antiphase equal power divider with four output ports and 90° phase delay in an anticlockwise sequence, as shown in Fig. 3. The parameter "L" connected to the four output ports is considered as a variable design parameter to optimize the phase of across the feed network. One should note that, since each "L" section has a 50 Ω characteristic impedance, its length variations do not impact the impedance matching of the feeding network.

IV. FSS Unit Cell Design

In order to reduce RCS, two different FSS cells (parameters are given in Fig. 4) with different reflection phase responses

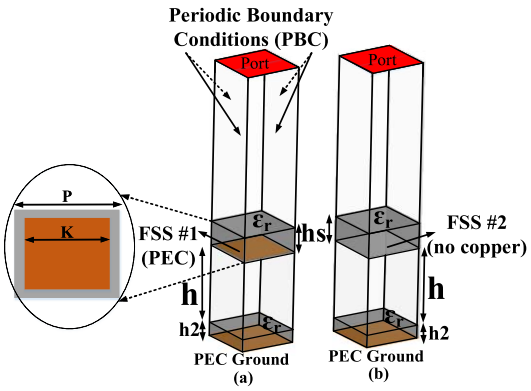

Fig. 4. Simulated models of the FSS unit cells. (a) FSS #1. (b) FSS #2 (P = 3.5 mm, K = 3.2 mm, h = 4. 8 mm, h2 = 0.787 mm, hs = 1.52 mm, and $\varepsilon r = 2.2$).

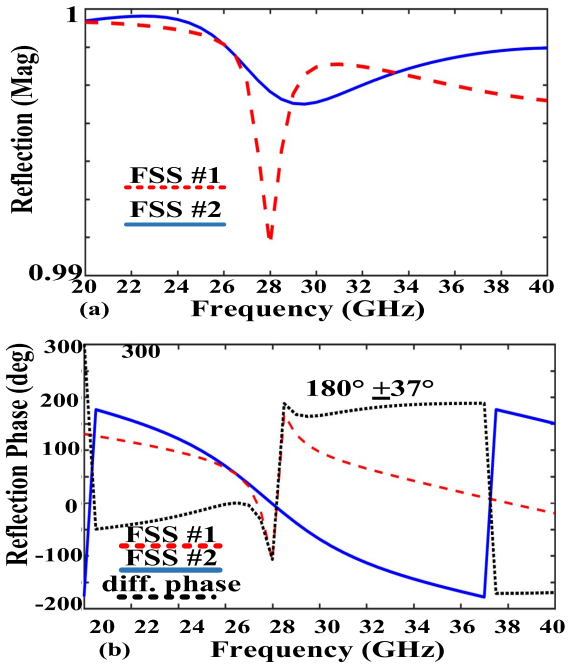

Fig. 5. Reflection coefficients of FSS units. (a) Magnitude. (b) Phase.

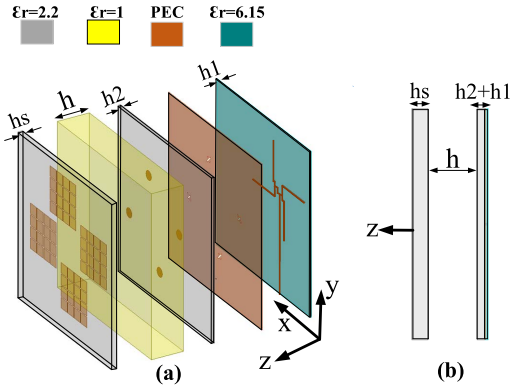

Fig. 6. (a) 3-D topology. (b) Side view of the FPCA (h1 = 0.25 mm, h2 = 0.787 mm, h = 4.8 mm, and hs = 1.52 mm).

are essential. With respect to modeling and analysis discussed in Section III, the unit cells are considered as a single box containing the metasurface, air gap, second substrate, and metal ground plate, as shown in Fig. 4. To fully study the reflection features of the FSS unit cells, the full-wave numerical analysis is carried out in ANSYS HFSS utilizing a unitary cell under proper periodic boundary conditions and floquet port excitation. Obviously, the unit cell analysis approach not only decreases the computation time but also accurately anticipates the reflection and transmission coefficients as compared to including the whole structure. A dielectric loss tangent of 0.0009 is assumed. The difference between FSS #1 and FSS #2 unit cells is only the copper patch, while all dimensions and materials are identical. For FSS #1, a copper patch is printed on the bottom surface of superstrate, as depicted in Fig. 4(a). The simulation results of reflection coefficients for the two FSS unit cells are shown in Fig. 5. From Fig. 5(a), it can be observed that the magnitudes of the reflection coefficient for both the FSS cells are higher than 0.99 which ensures the high gain based on the following [28]:

$$Dr = \frac{(1 + |\Gamma(f, \theta = 0)|)}{(1 - |\Gamma(f, \theta = 0)|)} \tag{3}$$

where Dr is the relative directivity on the broadside direction ($\theta = 0$) and Γ is the magnitude of the reflection coefficient. In addition, the half-power fractional bandwidth of highly reflecting superstrate with frequency-dependent reflection characteristics can be computed as follows [28]:

$$HPBW = \frac{\Delta f}{f_0} = \frac{\lambda}{2\pi h} \frac{1 - \Gamma}{\sqrt{\Gamma}}. \tag{4}$$

As one can be observed from (3), the directivity is based on the reflectivity (Γ) of the metasurface so that the directivity (Dr) increases significantly with reflectivity (Γ). Therefore, the high directivity is achieved with a greatly reflective screen. Although, from (4) it can be found out that the bandwidth is reduced as (Γ) increases.

One approach to address this problem is to optimize the reflectivity (phase and magnitude) using (1)–(4) [28]. After the optimization process by HFSS, the reflection phase of both the FSS unit cells and also the difference between those are computed [see Fig. 5(b)]. It can be observed that the phase difference of the reflected waves remains in the range 180° ± 37° from 28.2 to 48 GHz (52%). Therefore, a wideband RCS reduction (nearly 52%) for the proposed structure is expected.

V. Proposed FPC Antenna Design

To form the FPCA, the FSS metasurface is placed over the source antenna [shown in Fig. 3(a)] at an air gap of "h." In Fig. 6, different material properties of the proposed FPCA are given. Fig. 7 shows the top view of the FSS metasurface, where to fulfill the RCS reduction requirements, each FSS structure is formed by 4 × 4 FSS unit cells with an entire dimension of 14 × 14 mm^2. Note that the copper patches of FSS #1 are printed on the bottom surface of the superstrate.

The enhanced performance of the overall FPCA is controlled by different design parameters. First, by choosing a suitable air gap "h," the wide impedance bandwidth of the source antenna is conserved. Second, a gain increase is

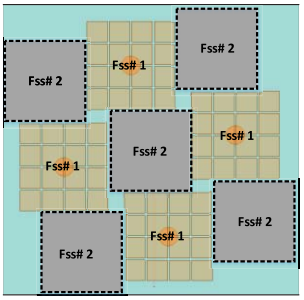

Fig. 7. Top view of the FSS metasurface including structures of FSS #1 and FSS #2 (each FSS structure is formed by 4 × 4 FSS unit cells).

achieved by the FPC formed by the metasurface and the ground plate. Third, to preserve the CP property of the source antenna, the appropriate arrangement of the FSS unit cell is required. Fourth, using the FSS metasurface backed by the ground plate, a reflective broadband RCS reduction is obtained. Evidently, it is complicated to optimize the four functions at the same time. Therefore, our purpose is to obtain a compromise between the above properties. The FSS metasurface is designed using the following procedure.

1) Design the FSS unit cell with reflecting properties to generate a broadband FPC and the highest magnitude to enhance directivity (Figs. 4 and 5)
2) Find the proper air gap "h" between the source antenna and the FSS metasurface to cover a preferable impedance bandwidth of the antenna (26–34 GHz).
3) Arrange the FSS unit cells in terms of the number and location at the bottom of the metasurface to fulfill the CP-wave requirements to preserve and expand the 3 dB AR bandwidth.
4) Suppress the broadband RCS by $180° \pm 37°$ reflection phase variations between adjacent FSS unit cells (FSS #1 and FSS #2). Note that FSS #2 should somehow behave to not deteriorate other factors generated by FSS #1 such as the impedance and CP bandwidths, and gain enhancement (see Figs. 4 and 5).
5) Optimize the parameter "L" with a characteristic impedance of 50 Ω to control the phases and manage an appropriate tradeoff between the four main overall performance factors: impedance and CP bandwidths, gain enhancement, and RCS reduction).

Fig. 8 compares the ANSYS HFSS's simulation results of the reflection coefficient, AR, and gain for both source antennae alone and the proposed FPCA with the metasurface. One should note that after optimization the air-gap height h, between the source antenna and the metasurface, is 4.8 mm (close to half a wavelength). It is seen in Fig. 8 that the impedance bandwidths of the source antenna and FPCA (with metasurface) are 25.6–34.5 GHz (29.6%) and 26.5–35 GHz (27.6%), respectively. They are close to each other because the air gap is approximately half a wavelength of free space.

The simulated 3 dB AR bandwidth for the proposed antenna at broadside is ranged from 26.5 to 32.9 GHz (21.5%). On the other hand, as shown in Fig. 8, the simulated 3 dB gain bandwidth for the source antenna is from 26.4 to 35 GHz (28%)

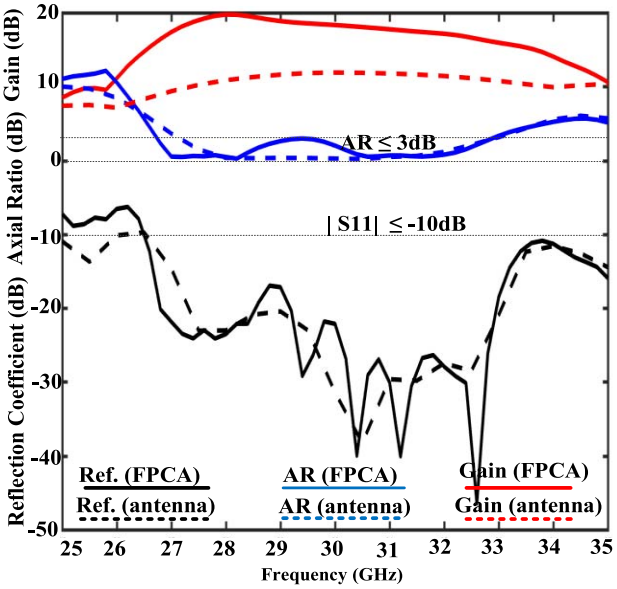

Fig. 8. Simulated reflection coefficient, AR, and gain for both the source antenna (without metasurface) and the FPCA (with metasurface).

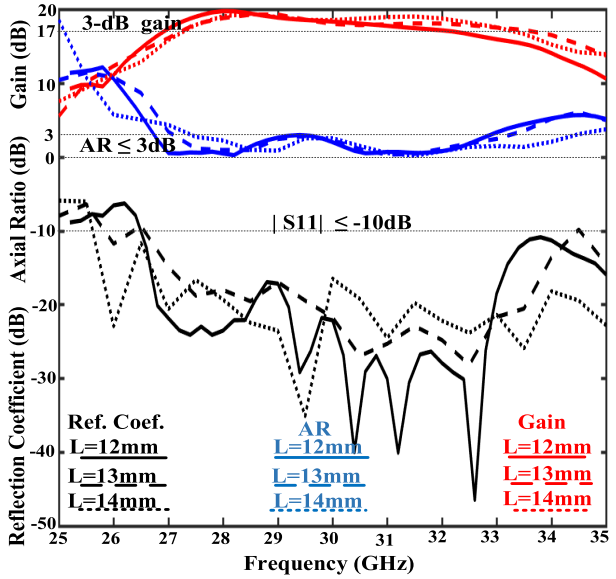

Fig. 9. Simulated reflection coefficient, AR, and gain for FPCA (with metasurface) for "L" parameter variations.

with the maximum gain of 12 dB at 29 GHz. The FPCA, with a peak gain of 20 dB at 28 GHz, has 3 dB gain bandwidth from 26.8 to 32.6 GHz (19.5%). At 28 GHz, the FSS metasurface enhances the gain by 10 dB. As noted previously, the parameter "L" gives a design freedom to optimize all performance factors.

As shown in Fig. 9, variations in the gain and impedance performances of the proposed antenna are not so significant with "L" variations. However, to make an appropriate decision concerning a good "L" value, the scattering behavior (monostatic RCS) for different values of "L" should be considered. As depicted in Fig. 10, it can be concluded that the monostatic RCS variations in the normal incidence for different values of "L" seem to be considerable. Therefore, based on

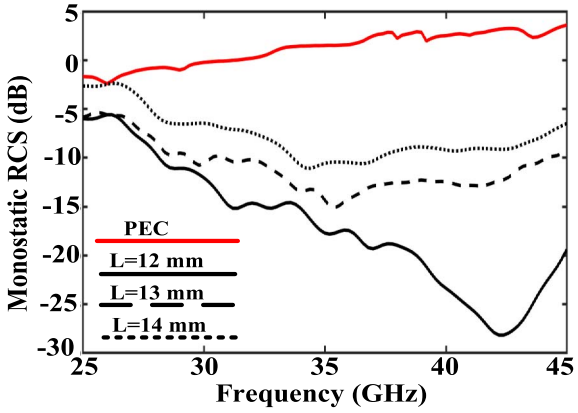

Fig. 10. Monostatic RCS comparison of the FPCA with both the proposed and PEC metasurface with "L" parameter variations.

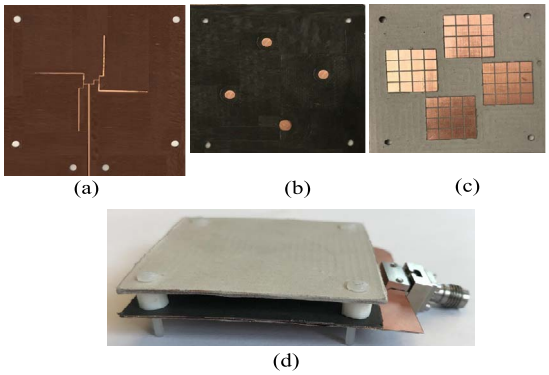

Fig. 11. Photograph of the assembled fabricated antenna. (a) Bottom view of the sequential feeding transition substrate of RO3006. (b) Top view of the second substrate of RT5880 showing the patch. (c) Bottom layer of the FSS metasurface of RT5880. (d) Proposed FPCA.

Fig. 10 and to satisfy the RCS suppression requirement, "L" is selected to be 12 mm.

VI. Fabrication and Measurement

In order to further verify the impedance, radiation, and scattering simulated performance of the proposed design, the FPCA is fabricated utilizing a common printed circuit board fabrication approach. The photograph of the assembled fabricated antenna is exhibited in Fig. 11. One should note that the source antenna is embedded inside a cavity formed by placing the FSS metasurface roughly 4.8 mm above it by four Nylon spacers. The reflection coefficient of the proposed FPCA is measured using an Agilent N5227A performance network analyzer (PNA) (10 MHz–67 GHz). A LP probe was employed to sequentially measure the electric field in two directions inside the anechoic chamber for obtaining the experimental results of the gain and radiation pattern.

The RHCP and LHCP fields and then AR of the proposed FPCA are computed by measured $E_\theta = |E_\theta|E_\theta$ and $E_\varphi = |E_\varphi|E_\varphi$ as follows [1]:

$$\vec{E}_{RHCP} = \frac{1}{\sqrt{2}}\left(\vec{E}_\theta + j\vec{E}_\varphi\right), \quad \vec{E}_{LHCP} = \frac{1}{\sqrt{2}}\left(\vec{E}_\theta - j\vec{E}_\varphi\right) \tag{5}$$

$$AR(\text{dB}) = 10log\left(\left|\frac{|\vec{E}_{RHCP}| + |\vec{E}_{LHCP}|}{|\vec{E}_{RHCP}| - |\vec{E}_{LHCP}|}\right|\right). \tag{6}$$

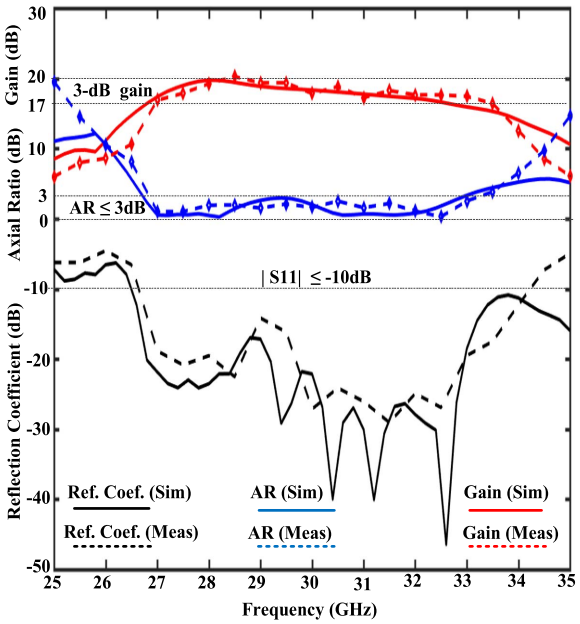

Fig. 12. Simulated and measured reflection coefficient, AR, and gain for FPCA (with metasurface).

The measured and simulated results of the realized gain, AR, and reflection coefficient are compared with each other, as exhibited in Fig. 12. It can be observed that there exist an excellent agreement between simulations and measurements so that the bandwidth of reflection coefficient ($|S_{11}| \leq -10$ dB) of the fabricated FPCA is 26.7–34.2 GHz (24.6%). The simulated and measured AR and gain at broadside are also shown in Fig. 12. The measured 3 dB AR bandwidth is 21%, expanding from 26.8 to 33.1 GHz, while the measured 3 dB gain bandwidth is 19.7%, ranging from 27.5 to 33.5 GHz with a peak gain of approximately 20 dBi at 28.5 GHz. The normalized simulations and measurements of RHCP and LHCP gain for the FPCA at $\varphi = 45°$ for three frequencies of 27.5, 30, and 33 GHz are demonstrated in Fig. 13. The maximum radiation all occurs at broadside orientation and there is a significant gain difference between the RHCP and LHCP in the main beam for the three frequencies. It is also found out that SLLs are increasing with a frequency that is inherited from the radiation features of the source antenna. In addition, the measured patterns have considerable resemblance trends with simulated ones. To validate the effectiveness of the proposed design on RCS suppression, the FPCA is terminated with a matching load and mounted vertically on a foam platform. Two horn antennas, as transmitter and receiver, are connected to an E8364B PNA (10 MHz–50 GHz). Note that, due to a set of difficulties associated with bistatic measurements, only backscatter results (under normal incidence) of the proposed FPCA is experimentally measured in the anechoic chamber of Concordia University. Meanwhile, the FPCA terminated with a matching load is placed far enough from the horn antennas inside the anechoic chamber in the far field of the horn antennas to ensure a plane wave impingement. One should note that to calculate the RCS reduction, measurement of the scattering waves from the metallic metasurface with

TABLE I

COMPARISON BETWEEN THE PROPOSED STRUCTURE WITH THE SIMILAR DESIGNS IN REFERENCE

Year/ Reference	Impedance B.W. (GHz) and (%)	CP property/ Relative 3-dB AR B.W. (%)	Relative 3-dB Gain B.W. (GHz)	Peak Gain (dB)	RCS Reduction B.W. (%)
2014/ [22]	11.2-12.0 (6.9%)	LP/ -	3.7	13.5	80
2015/ [24]	9.0-9.9 (9.5%)	LP/ -	17.3	13	54.5
2015/ [30]	9.9-10.9 (9.6%)	LP/ -	N/A	10.8	85.7
2016/ [31]	5.4-5.8 (7.1%)	LP/ -	7.5	9.5	66.7
2016/ [32]	9.5-10.9 (13.7%)	LP/ -	7.0	11.0	133.3
2018/ [33]	9.4-11.3 (18.3%)	LP/ -	16.6	10.5	76.9
Proposed	26.7-34.2 (24.6%)	CP/ 21	19.7	20	52

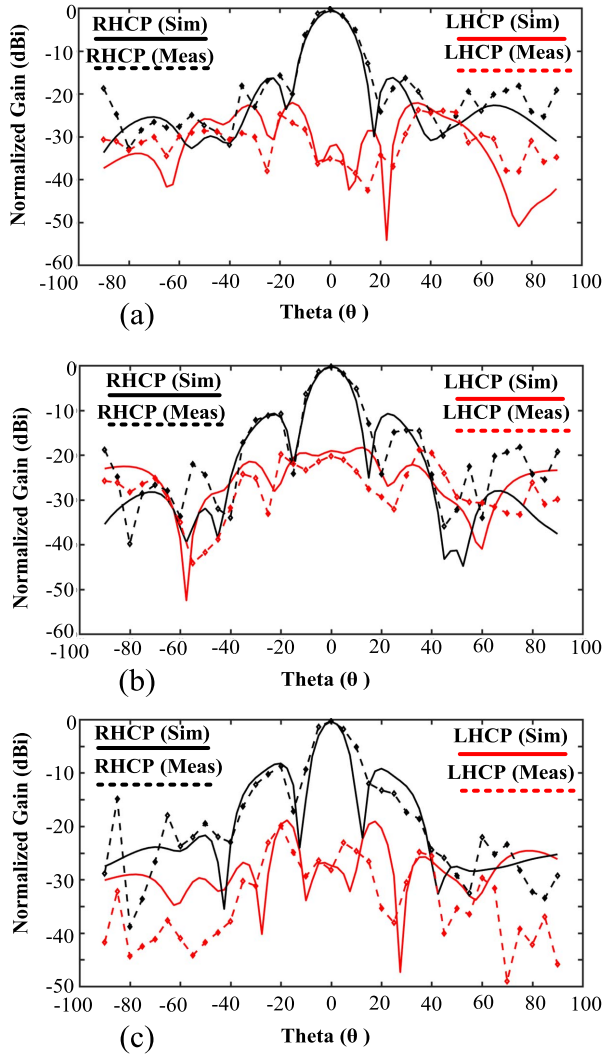

Fig. 13. Normalized simulations and measurements of RHCP and LHCP gain at $\varphi = 45°$ for the FPCA at three frequencies of (a) 27.5, (b) 30, and (c) 33 GHz.

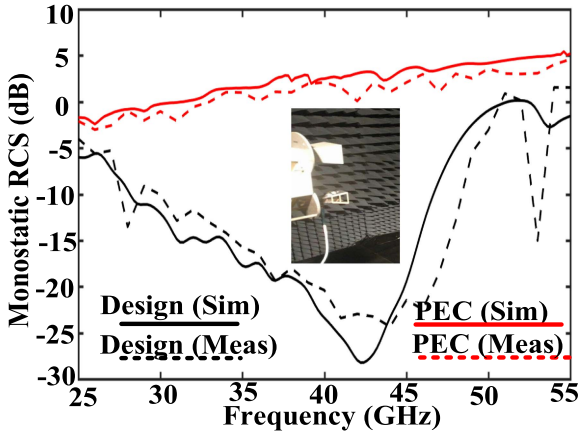

Fig. 14. Simulated and measured monostatic RCS of the proposed FPCA and the PEC metasurface with the same size under normal incidence, the photograph of two kinds of horn antennas used for transmitting and receiving.

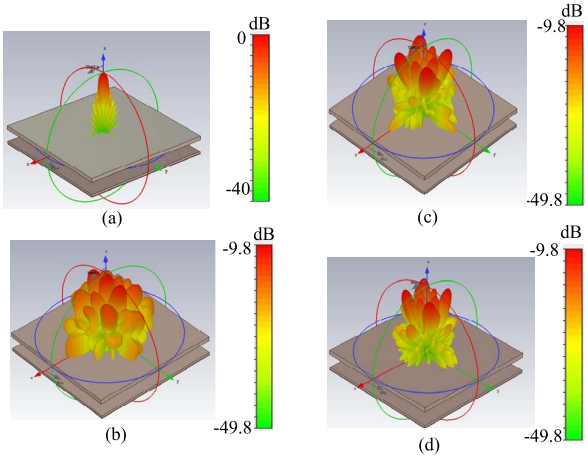

Fig. 15. 3-D RCS pattern of the FPCA terminated with the matching load under normal incidence for (a) particular case of the metallic plate, the proposed metasurface at (b) 30, (c) 35, and (d) 42.2 GHz. (Plots are normalized with a metallic plate.)

the identical size are essential, as well. The measured and simulated monostatic RCS of both the FPCA and the metallic metasurface with the same size under normal incidence are shown in Fig. 14. It can be observed that considerable RCS reduction is obtained from 28 to 48 GHz with a relative bandwidth of 52%, covering the in-band and out-band. The 3-D RCS pattern of the FPCA at different frequencies of 30, 35, and 42.2 GHz are shown in Fig. 15.

In comparison with 3-D RCS pattern of the metallic metasurface with the same size [see Fig. 15(a)], it can be concluded that the grating lobes are greatly diminished by the proposed metasurface and scattered fields are distributed more uniformly

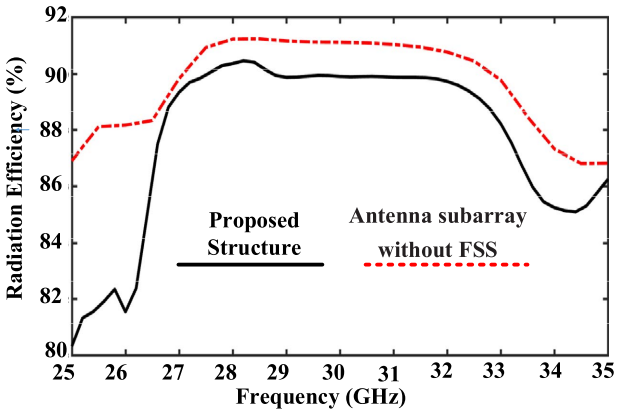

Fig. 16. Simulated radiation efficiency of 2×2 antenna subarrays without FSS and the proposed structure versus frequency.

in angular space. The 9.8 dB drop in the amplitude of the reference metallic plate peak is a good relevant evidence to prove this claim. Note that an absolute cancellation is not obtained since the phase difference between both FSS structures does not preserve precisely the 180° and is varying in the range $180° \pm 37°$. The simulated results of radiation efficiency of 2×2 antenna subarrays without FSS and the proposed structure are depicted in Fig. 16. It can be observed that the radiation efficiency for both cases is around 90% on the frequency band of interest. In order to further understand the modified characteristics of the proposed FPCA, a comparative study of the proposed structure with some recently published work is given in Table I. It is obvious that the proposed structure provides the broader 3 dB gain and impedance bandwidths, and more gain enhancement along with CP property.

In addition, RCS reduction is nearly started from operating frequency band of the FPCA, covering 52%. These major characteristics acquired simultaneously by the proposed FPCA are missing in other relevant work with respect to Table I.

VII. Conclusion

A broadband CP antenna with high gain and low-RCS employing an FSS metasurface at the *Ka*-band is presented in this paper. The RCS reduction is obtained through phase cancellation of two types of FSS structures which are formed by 4×4 FSS unit cells. The new FSS unit cell consists of three layers terminated by the metallic plate of the source antenna. At a given frequency, this approach prevents any deterioration in both radiation performance and scattering property of the FPCA. Also, a microstrip slot array excited by a sequentially rotated feeding network is applied as the source antenna to illuminate the FSS metasurface. Experimental and simulated results validated the design approach and indicated that by employing an FSS metasurface, the structure gain is enhanced by at least 7 dB as compared with the source antenna without the metasurface. Furthermore, the 3 dB gain, impedance ($|S11| \leq -10$ dB), AR $\leq$3 dB, and monostatic RCS reduction bandwidths are 19.7%, 24.6%, 21%, and 52%, respectively. A main advantage of the proposed approach is introducing a new alternative scheme to solve conflict requirements between radiation and scattering performance of a source antenna. The proposed antenna can be used in different applications including stealth platforms in which RCS suppression and gain enhancement are both necessary.

References

[1] M. Akbari, S. Gupta, M. Farahani, A. R. Sebak, and T. A. Denidni, "Gain enhancement of circularly polarized dielectric resonator antenna based on FSS superstrate for MMW applications," *IEEE Trans. Antennas Propag.*, vol. 64, no. 12, pp. 5542–5546, Dec. 2016.

[2] M. Akbari, H. A. Ghalyon, M. Farahani, A.-R. Sebak, and T. A. Denidni, "Spatially decoupling of CP antennas based on FSS for 30-GHz MIMO systems," *IEEE Access.*, vol. 5, pp. 6527–6537, Apr. 2017.

[3] M. Akbari, M. Farahani, A.-R. Sebak, and T. A. Denidni, "Ka-band linear to circular polarization converter based on multilayer slab with broadband performance," *IEEE Access.*, vol. 5, pp. 17927–17937, Aug. 2017.

[4] Y. J. Lee, J. Yeo, R. Mittra, and W. S. Park, "Application of electromagnetic bandgap (EBG) superstrates with controllable defects for a class of patch antennas as spatial angular filters," *IEEE Trans. Antennas Propag.*, vol. 53, no. 1, pp. 224–235, Jan. 2005.

[5] C. Cheype, C. Serier, M. Thevenot, T. Monediere, A. Reineix, and B. Jecko, "An electromagnetic bandgap resonator antenna," *IEEE Trans. Antennas Propag.*, vol. 50, no. 9, pp. 1285–1290, Sep. 2002.

[6] A. R. Weily, K. P. Esselle, T. S. Bird, and B. C. Sanders, "High gain circularly polarised 1-D EBG resonator antenna," *Electron. Lett.*, vol. 42, no. 18, pp. 1012–1013, Apr. 2006.

[7] G. Zhao, Y.-C. Jiao, F. Zhang, and X. Yang, "High gain circularly polarized antenna using sub-wavelength resonant cavity," *J. Electromagn. Waves Appl.*, vol. 24, no. 1, pp. 33–40, Aug. 2010.

[8] A. Pirhadi, M. Hakkak, F. Keshmiri, and R. K. Baee, "Design of compact dual band high directive electromagnetic bandgap (EBG) resonator antenna using artificial magnetic conductor," *IEEE Trans. Antennas Propag.*, vol. 55, no. 6, pp. 1682–1690, Jun. 2007.

[9] M. U. Afzal, K. P. Esselle, and B. A. Zeb, "Dielectric phase-correcting structures for electromagnetic band gap resonator antennas," *IEEE Trans. Antennas Propag.*, vol. 63, no. 8, pp. 3390–3399, Aug. 2015.

[10] M. U. Afzal and K. P. Esselle, "A low-profile printed planar phase correcting surface to improve directive radiation characteristics of electromagnetic band gap resonator antennas," *IEEE Trans. Antennas Propag.*, vol. 64, no. 1, pp. 276–280, Jan. 2016.

[11] D. R. Jackson and A. A. Oliner, "A leaky-wave analysis of the high-gain printed antenna configuration," *IEEE Trans. Antennas Propag.*, vol. AP-36, no. 7, pp. 905–910, Jul. 1988.

[12] T. Zhao, D. R. Jackson, J. T. Williams, H.-Y. D. Yang, and A. A. Oliner, "2-D periodic leaky-wave antennas—Part I: Metal patch design," *IEEE Trans. Antennas Propag.*, vol. 53, no. 11, pp. 3505–3514, Nov. 2005.

[13] T. Zhao, D. R. Jackson, and J. T. Williams, "2-D periodic leaky-wave antennas—Part II: Slot design," *IEEE Trans. Antennas Propag.*, vol. 53, no. 11, pp. 3515–3524, Nov. 2005.

[14] M. Thevenot, C. Cheype, A. Reineix, and B. Jecko, "Directive photonic-bandgap antennas," *IEEE Trans. Microw. Theory Techn.*, vol. 47, no. 11, pp. 2115–2122, Nov. 1999.

[15] Y. Ge, K. P. Esselle, and T. S. Bird, "The use of simple thin partially reflective surfaces with positive reflection phase gradients to design wideband, low-profile EBG resonator antennas," *IEEE Trans. Antennas Propag.*, vol. 60, no. 2, pp. 743–750, Feb. 2012.

[16] R. Gardelli, M. Albani, and F. Capolino, "Array thinning by using antennas in a Fabry–Pérot cavity for gain enhancement," *IEEE Trans. Antennas Propag.*, vol. 54, no. 7, pp. 1979–1990, Jul. 2006.

[17] M. Diblanc, E. Rodes, E. Arnaud, M. Thevenot, T. Monediere, and B. Jecko, "Circularly polarized metallic EBG antenna," *IEEE Microw. Wireless Compon. Lett.*, vol. 15, no. 10, pp. 638–640, Oct. 2005.

[18] S. A. Muhammad, R. Sauleau, L. Le Coq, and H. Legay, "Self-generation of circular polarization using compact Fabry–Pérot cavity antennas," *IEEE Antenna Wireless Propag. Lett.*, vol. 10, pp. 907–910, Sep. 2011.

[19] R. Orr, G. Goussetis, and V. Fusco, "Design method for circularly polarized Fabry–Pérot cavity antennas," *IEEE Trans. Antennas Propag.*, vol. 62, no. 1, pp. 19–26, Jan. 2014.

[20] S. A. Muhammad, R. Sauleau, G. Valerio, L. Le Coq, and H. Legay, "Self-polarizing Fabry–Pérot antennas based on polarization twisting element," *IEEE Trans. Antennas Propag.*, vol. 61, no. 3, pp. 1032–1040, Mar. 2013.

[21] Z. G. Liu, Y. X. Guo, and Z. X. Cao, "Compact low-profile circularly polarized Fabry–Pérot resonator antenna fed by linearly polarized microstrip patch," *IEEE Antenna Wireless Propag. Lett.*, vol. 15, pp. 524–527, Sep. 2016.
[22] W. Pan, C. Huang, P. Chen, X. Ma, C. Hu, and X. Luo, "A low-RCS and high-gain partially reflecting surface antenna," *IEEE Trans. Antennas Propag.*, vol. 62, no. 2, pp. 945–949, Feb. 2014.
[23] C. Huang, W. Pan, X. Ma, and X. Luo, "A frequency reconfigurable directive antenna with wideband low-RCS property," *IEEE Trans. Antennas Propag.*, vol. 64, no. 3, pp. 1173–1178, Mar. 2016.
[24] Y. J. Zheng, J. Gao, X. Y. Cao, S. J. Li, and W. Q. Li, "Wideband RCS reduction and gain enhancement microstrip antenna using chessboard configuration superstrate," *Microw. Opt. Technol. Lett.*, vol. 57, no. 7, pp. 1738–1741, Jul. 2015.
[25] K. Kandasamy, B. Majumder, J. Mukherjee, and K. P. Ray, "Low-RCS and polarization-reconfigurable antenna using cross-slot-based metasurface," *IEEE Antennas Wireless Propag. Lett.*, vol. 14, pp. 1638–1641, Aug. 2015.
[26] P. Yang, F. Yan, F. Yang, and T. Dong, "Microstrip phased array in-band RCS reduction with a random element rotation technique," *IEEE Trans. Antennas Propag.*, vol. 64, no. 6, pp. 2513–2518, Jun. 2016.
[27] Y. Liu, K. Li, Y. Jia, Y. Hao, S. Gong, and Y. J. Guo, "Wideband RCS reduction of a slot array antenna using polarization conversion metasurfaces," *IEEE Trans. Antennas Propag.*, vol. 64, no. 1, pp. 326–331, Jan. 2016.
[28] A. P. Feresidis and J. C. Vardaxoglou, "High gain planar antenna using optimised partially reflective surfaces," *IEE Proc.-Microw., Antennas Propag.*, vol. 148, no. 6, pp. 345–350, Dec. 2001.
[29] M. Akbari, S. Gupta, M. Farahani, A. R. Sebak, and T. A. Denidni, "Analytic study on CP enhancement of millimeter wave DR and patch subarray antennas," *Int. J. RF Microw. Comput.-Aided Eng.*, vol. 27, no. 1, p. e21053, 2017.
[30] Y. Zheng, J. Gao, X. Cao, Z. Yuan, and H. Yang, "Wideband RCS reduction of a microstrip antenna using artificial magnetic conductor structures," *IEEE Antennas Wireless Propag. Lett.*, vol. 14, pp. 1582–1585, Aug. 2015.
[31] Y. Zhao *et al.*, "Broadband low-RCS metasurface and its application on antenna," *IEEE Trans. Antennas Propag.*, vol. 64, no. 7, pp. 2954–2962, Jul. 2016.
[32] W.-Q. Li, X.-Y. Cao, J. Gao, Z. Zhang, and L.-L. Cong, "Broadband RCS reduction and gain enhancement microstrip antenna using shared aperture artificial composite material based on quasi-fractal tree," *IET Microw., Antennas Propag.*, vol. 10, no. 4, pp. 370–377, Mar. 2016.
[33] Y. Zheng *et al.*, "Wideband gain enhancement and RCS reduction of Fabry–Pérot resonator antenna with chessboard arranged metamaterial superstrate," *IEEE Trans. Antennas Propag.*, vol. 66, no. 2, pp. 590–599, Feb. 2018.

Saman Zarbakhsh (S'18) was born in Tehran, Iran, in 1984. He received the B.Sc. degree in electrical engineering from the Azad University of South Tehran, Tehran, Iran, in 2007, and the M.Sc. degree in electrical engineering from Urmia University, Urmia, Iran, in 2010. He is currently pursuing the Ph.D. degree with the Electrical and Computer Engineering Department, Concordia University, Montreal, QC, Canada.

Since 2015, he has been a Research Assistant with Concordia University. His current research interests include phased array antennas, MIMO antenna, radar cross section reduction, circularly polarized (CP) antenna, high-gain antenna, reconfigurable liquid metal antenna, periodic structures, frequency selective surface, and linearly polarized-to-CP polarizer.

Mr. Zarbakhsh was a recipient of the International Tuition Award of Excellence in 2015.

Mohammad Akbari (M'15) received the B.Sc. degree in electrical and telecommunications engineering from the University of Shahid Bahonar, Kerman, Iran, in 2007, the M.Sc. degree in electrical engineering from the University of Urmia, Urmia, Iran, in 2011, and the Ph.D. degree in electrical and computer engineering from Concordia University, Montreal, QC, Canada, in 2018.

From 2014 to 2018, he was a Research and Teaching Assistant with Concordia University. He is currently a Post-Doctoral Fellow with the Institute National de la Recherché, Montreal. He has authored or co-authored of approximately 80 peer-reviewed scientific journals and international conference papers. He holds one patent. His current research interests include metasurface and metamaterials, high-gain millimeter-wave antenna arrays for millimeter-wave (5G) wireless communications, miniaturization approaches, mutual coupling reduction techniques, reconfigurable, phase array, dielectric resonator and wearable antennas, ridge gap waveguide feeding networks, sequential feeding techniques, radar cross section reduction, and polarizer ultrawideband technology.

Dr. Akbari was a recipient of the Concordia University International Tuition Fee Remission Award in 2014, the Graduate Concordia Merit Scholarship in 2016, and the Accelerator Award in 2017. He served as a Reviewer for the IEEE ANTENNAS AND PROPAGATION SOCIETY'S JOURNALS AND MAGAZINE.

Fereshteh Samadi (S'18) was born in Marand, Iran, in 1990. She received the bachelor's degree (Hons.) in electrical and electronic engineering from the University of Tabriz, Tabriz, Iran, in 2012, and the M.Sc. degree in electrical engineering from the University of Urmia, Urmia, Iran, in 2014. She is currently pursuing the Ph.D. degree in electrical engineering with the University of Concordia, Montreal, QC, Canada.

Her current research interests include antennas and phased array antennas, scattering and beamforming, and antennas for wireless communications and medical applications.

Abdel-Razik Sebak (F'10) received the B.Sc. degree (Hons.) in electrical engineering from Cairo University, Cairo, Egypt, in 1976, the B.Sc. degree in applied mathematics from Ain Shams University, Cairo, in 1978, and the M.Eng. and Ph.D. degrees in electrical engineering from the University of Manitoba, Winnipeg, MB, Canada, in 1982 and 1984, respectively.

From 1984 to 1986, he was with Canadian Marconi Company, where he was involved in the design of microstrip phased array antennas. From 1987 to 2002, he was a Professor with the Department of Electronics and Communication Engineering, University of Manitoba. He is currently a Professor with the Department of Electrical and Computer Engineering, Concordia University, Montreal, QC, Canada. His current research interests include phased array antennas, millimeter-wave antennas and imaging, computational electromagnetics (EMs), and interaction of EM waves with engineered materials and bio-EMs.

Dr. Sebak is a member of the Canadian National Committee of International Union of Radio Science (URSI) Commission B. He was a recipient of the 2000 and 1992 University of Manitoba Merit Award for outstanding Teaching and Research, the 1994 Rh Award for Outstanding Contributions to Scholarship and Research, and the 1996 Faculty of Engineering Superior. He served as the Chair for the IEEE Canada Awards and Recognition Committee from 2002 to 2004 and the Technical Program Chair for the 2002 IEEE CCECE Conference and the 2006 URSIANTEM Symposium. He is the Technical Program Co-Chair for the 2015 IEEE ICUWB Conference.